Calibration of the δ^{18}O isotopic paleothermometer for central Greenland, using borehole temperatures

KURT M. CUFFEY* AND RICHARD B. ALLEY,

Earth System Science Center and Department of Geosciences, The Pennsylvania State University, University Park, Pennsylvania 16802, U.S.A.

PIETER M. GROOTES,

Quaternary Isotope Laboratory, University of Washington, Seattle, Washington 98195, U.S.A.

JOHN M. BOLZAN,

Byrd Polar Research Center, The Ohio State University, Columbus, Ohio 43210, U.S.A.

SRIDHAR ANANDAKRISHNAN

Earth System Science Center and Department of Geosciences, The Pennsylvania State University, University Park, Pennsylvania 16802, U.S.A.

ABSTRACT. We calibrate the δ^{18}O paleothermometer for central Greenland using borehole temperatures, a thermal model forced by a measured δ^{18}O record and a formal inverse technique. The calibration is determined mostly by temperature fluctuations of the last several centuries, including the Little Ice Age. Results are generally insensitive to model variables, including initial condition, basal boundary condition, parameterization of snow thermal properties, ice thickness and likely errors in temperature and isotope measurements. Results of this borehole calibration also seem to be in agreement with modern spatial gradients of δ^{18}O and temperature. We suggest that calibrations of isotopic paleothermometers using borehole temperatures are a useful paleoclimate tool, because they are independent of spatial gradients and include the effects of prehistoric temperatures over ice sheets.

INTRODUCTION

Ice-core paleoclimate studies rely on stable-isotope ratios, particularly δ^{18}O, to provide continuous and detailed temperature records. The relationship between δ^{18}O and temperature T, for time t, is assumed to be linear

$$\delta^{18}O(t) = aT(t) + b \tag{1}$$

where a and b are coefficients that do not vary with time.

Even if Equation (1) is not strictly valid (Jouzel and Merlivat, 1984), it is still important to ask what values of these coefficients are most appropriate since this relationship is in widespread use. There are two commonly used methods for finding values of these coefficients (Robin, 1983). The first is the spatial gradient method, which assumes that

$$\delta^{18}O\big(T(t, \phi_0, \omega_0)\big) = \delta^{18}O\big(T(t_0, \phi, \omega)\big) \tag{2}$$

where t_0 is the present, ϕ and ω are latitude and longitude, and the coring site has location (ϕ_0, ω_0). One estimates the spatial relationship, $\delta^{18}O\big(T(t_0, \phi, \omega)\big)$, by measuring and correlating δ^{18}O and temperature at a variety of locations. The slope and intercept of the correlation line provide estimates of a and b, respectively. Peel and others (1988) have shown that the assumption, Equation (2), is incorrect in one case. The second method is time-series analysis of histories of recent temperature and δ^{18}O values. Time-series methods may give spurious results because detailed temperature records and isotope records are usually not available for the same location. Moreover, instrumental temperature records are necessarily of short duration and hence contain no information about low-frequency climate fluctuations.

The modern temperature–depth distribution in polar ice sheets is the result of the integrated response to past temperature and accumulation-rate changes. This makes possible a third method for calibrating the isotopic paleothermometer, if both a vertical temperature profile and an isotopic record are available for the same site; one can use a thermal model to determine values of a and b that generate a surface-temperature history which minimizes error between a solution of the model equations and a measured temperature profile (Paterson and Clarke, 1978).

* Present address: Department of Geological Sciences, AJ-20, University of Washington, Seattle, Washington 98195, U.S.A.

Here, we present results of a borehole temperature-based calibration of the $\delta^{18}O$ paleothermometer for the Greenland Ice Sheet Project II (GISP2) site in central Greenland and we argue that such calibrations are a useful tool for paleoclimatology. In addition, we present details of our thermal model and the inverse problem, examine the temporal range of applicability of our results, compare our results with modern spatial gradients of $\delta^{18}O$ and temperature, and quantify the sensitivity of our results to model inputs for which the true value is not known. We allow three parameters to vary in our inversion: the two constant coefficients in Equation (1) and the initial surface temperature. Our inversion seeks to minimize the model mean-square-error, E_{ms}, defined as

$$E_{ms} = \frac{1}{N} \sum_{p=1}^{p=N} (T_p - \Theta_p)^2 \qquad (3)$$

where T are modeled temperatures, Θ are measured borehole temperatures and N is the number of grid points. We have already presented preliminary results in Cuffey and others (1992).

METHODS

We convert isotopic records into a history of ice-sheet surface temperatures using Equation (1). We then calculate a temperature–depth profile, using a forward numerical model forced with these surface temperatures. Comparison with measured borehole temperatures allows us to invert for best-fit values of a and b in Equation (1). This inversion is done for a 1340 year record of $\delta^{18}O$ ending in AD 1989.

Measured temperatures

We use the temperature–depth profile measured by Alley and Koci (1990) in a 217 m deep borehole at the GISP2 site near the summit of the Greenland ice sheet. Alley and Koci found the shape of the measured profile to be reproducible to $\pm 0.01°C$, although the absolute value of the temperatures was consistently offset by 0.035°C for two different factory-calibrated thermistors. Temperature gradients in the borehole are $\leq 0.04°C\,m^{-1}$, less than the adiabatic lapse-rate of air at these temperatures. In addition, the borehole is narrow, limiting the potential size of convection cells. Convective disturbance of the borehole-temperature profile is therefore unlikely (Diment, 1967). A repeat measurement of the borehole temperatures 1 year later by Alley and others confirmed that the trend was undisturbed. For both years, we observed that the thermistors' resistance values were stable during measurement. Finally, the error resulting from distortion of the temperature distribution in the ice due to the presence of the air-filled borehole is insignificant for these low gradients (Sanderson, 1977). For all these reasons, we consider the borehole-temperature profile to reflect accurately the temperatures in the surrounding ice.

The model

Our thermal model is a one-dimensional finite-difference equation, similar to that used by Johnsen (1977),

Paterson and Clarke (1978), Bolzan (1985) and Alley and Koci (1990). Thermal energy per unit volume changes with time as (Malvern, 1969, p. 228–30)

$$\rho c \frac{\partial T}{\partial t} = \frac{\partial}{\partial z}\left[k \frac{\partial T}{\partial z}\right] - \rho c w \frac{\partial T}{\partial z} + \sigma : \dot{\epsilon} + \dot{S}$$

$$t_i < t < t_0, \quad 0 < z < 600 \qquad (4)$$

with boundary and initial conditions:

$$T(t = t_i, z) = T_i(z) \qquad 0 < z < 600 \qquad (5)$$

$$T_i(0) = \Delta + \bar{T}_s(a, b) \qquad (6)$$

$$T(t, z = 600) = T_{600}(\Delta, a, b) = T_i(0) + 0.09$$
$$t_i < t < t_0 \qquad (7)$$

$$T(t, z = 0) = T_s(t) = \frac{1}{a}\left[\delta^{18}O(t) - b\right]$$
$$t_i < t < t_0 \qquad (8)$$

where ρ is ice/firn density, c is heat capacity, T is temperature, t is time, t_i and t_0 correspond respectively to the years AD 649 and AD 1989, z is depth (0 at the ice-sheet surface, increasing downward), k is thermal conductivity, w is vertical velocity, σ is the stress tensor, $\dot{\epsilon}$ is the strain-rate tensor, and : indicates the inner product. $\dot{S}$ is the rate of energy production due to non-mechanical sources. The first three terms on the righthand side of Equation (4) account for heat transfer by conduction and advection and heat generation due to mechanical work during strain. Values for heat capacity are taken from Yen (1981, p. 13, table 2). For thermal conductivity, we use empirical data for firn densities $\rho < 750\,kg\,m^{-3}$ (Yen, 1981, p. 16, equation 35). For $\rho > 750\,kg\,m^{-3}$, we use empirical k values for pure ice (Yen, 1981, p. 15, equation 33), and a theoretical extrapolation for dense firn (Yen, 1981, p. 17, equation 37).

The initial temperature, $T_i(z)$, is a steady-state profile for an accumulation rate $\dot{b} = 0.24\,m\,a^{-1}$ and surface temperature $T_i(0)$. Equation (6) expresses $T_i(0)$ as an offset, Δ, from the average temperature during the model run, $\bar{T}_s(a, b)$, which is a function of the coefficients in Equation (1). Note that $\Delta > 0$ indicates the average temperature over the last 1340 year was less than that during the preceding years. We have shown that Δ probably falls in the range 0.65–0.90°C, with a most probable value of 0.79°C (Cuffey and others, 1992). This is similar to the result of Dahl-Jensen and Johnsen (1986), suggesting a Medieval Warm Period of this magnitude at Dye 3. Because the shape of the steady-state profile is fixed, T_{600} is uniquely determined by $T_i(0)$ (Equation (7)).

The remaining terms in Equation (4) are given by:

$$\sigma : \dot{\epsilon} = \sigma_z(\dot{\epsilon}_{z,d} + \dot{\epsilon}_{z,f}) + \sigma_x \dot{\epsilon}_x \qquad (9)$$

$$\dot{\epsilon}_{z,f} = -\dot{\epsilon}_x = \frac{-\dot{b}}{h_i} = A\sigma_d^3 \qquad (10)$$

$$\dot{\epsilon}_{z,d} = \frac{1}{\rho}\frac{D\rho}{Dt} = \frac{1}{\rho}\left(\frac{\partial \rho}{\partial t} + w\frac{\partial \rho}{\partial z}\right) = \frac{w}{\rho}\frac{\partial \rho}{\partial z} \qquad (11)$$

$$\sigma_z = g \int_0^z \rho\,dz = \sigma_x + 2\sigma_d \qquad (12)$$

$$w(z) = \frac{\rho \dot{b}}{\rho_i} + \int_0^z (\dot{\epsilon}_{z,d} + \dot{\epsilon}_{z,f})\,dz \qquad (13)$$

$$\dot{S} = \dot{S}_L + \dot{S}_g \approx 0. \qquad (14)$$

Here, σ_z is vertical stress and σ_x is horizontal stress normal to the ice divide (i.e. east–west) and $\dot{\epsilon}_x$ is the horizontal longitudinal strain rate in this direction. We partition the vertical longitudinal strain rate into components due to firn densification, $\dot{\epsilon}_{z,d}$, and flow divergence, $\dot{\epsilon}_{z,f}$. We assume plane strain in vertical planes normal to the ice divide, so no terms appear for the north–south horizontal direction. Because our model includes only the top 20% of the ice thickness and because GISP2 is only 30 km west of the ice divide, we neglect the work terms involving shear deformation, which are orders of magnitude less at these depths and low surface slopes. Note that the product $\sigma_z \dot{\epsilon}_{z,d}$ in Equation (9) gives the rate of heat dissipation due to work done moving grains closer together in the densification process, while the sum of the other two terms in Equation (9) gives the rate of heat dissipation due to the flow-divergence strain.

Incompressibility requires that the strain rates due to flow divergence sum to zero (Equation (10)). We assume that $\dot{\epsilon}_{z,f}$ has a constant value equal to the mean annual ice-equivalent accumulation rate, $\dot{b}$, divided by the ice-equivalent thickness, $h_i = 3100$ m (Hodge and others, 1990). We also assume power-law flow ($n = 3$) to write $\dot{\epsilon}_{z,f}$ in terms of the vertical longitudinal deviatoric stress, σ_d, and the usual flow-law pre-factor, A, taken from Paterson (1981, p. 39) for a temperature of $-30°$C.

In Equation (11), we write the vertical strain rate due to firn densification in terms of the material derivative of density ($D\rho/Dt$) and assume that the density at a given depth does not change through time. Equation (12) expresses the balance of forces; the vertical normal stress equals the weight of overburden and the sum of the longitudinal deviatoric stresses vanishes. The vertical velocity equals the snowfall rate at the surface and decreases with depth as the integral of the vertical strain rate (Equation (13)).

Finally, we assume that thermal energy released by non-mechanical sources is negligible (Equation (14)). At locations with frequent surface melt, the latent heat released upon refreezing of meltwater at depth ($\dot{S}_L$) can dominate the temperature structure (Paterson and Clarke, 1978). The paucity of inferred melt layers in the GISP2 ice cores (Alley and others, 1991) indicates we can neglect this term. Another source of thermal energy is the elimination of surface area during ice-grain growth ($\dot{S}_g$). We neglect this term, too, based on the following argument. The surface area of grain boundaries per volume of ice, A_{grains}, is approximately half the area of each grain (because each surface is largely shared by neighbouring grains) times the number of grains per volume. For spherical grains of radius r, $A_{grains} \approx 1.5/r$. The rate of energy release is the product of surface energy associated with the ice–ice boundaries ($\gamma_i = 0.065$ J m^{-2}; Hobbs, 1974, p. 440) and rate of elimination of grain-boundary area, or, for a steady distribution of grain-size with depth,

$$\dot{S}_g = -\gamma_i w \frac{dA_{grains}}{dz} \approx \frac{1.5\gamma_i w}{r^2} \frac{dr}{dz}. \quad (15)$$

$\dot{S}_g$ will be a maximum for shallow ice, where $r \approx 10^{-3}$ m, and r increases by approximately 1 mm per hundred meters, giving a temperature change at a rate of $(\partial T/\partial t) = (1/\rho c)\dot{S}_g \leq 1.2 \times 10^{-7}$ °C year^{-1}, which is more than
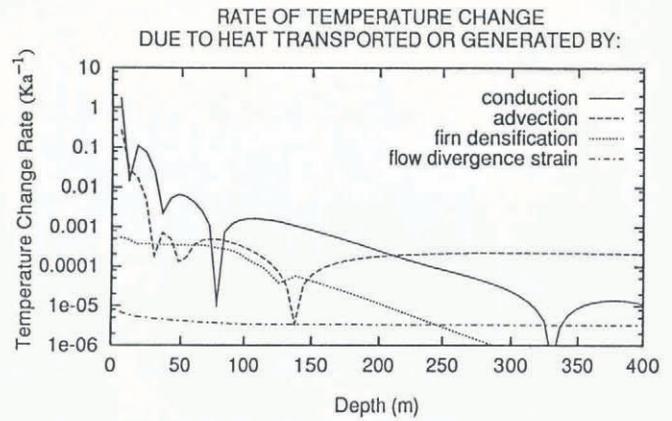
Fig. 1. Contribution of different heat-transfer and generation mechanisms to rate of temperature change $(K\,a^{-1})$ in the ice sheet, calculated for AD 1989. Absolute values for temperature-change rate were taken to make possible the logarithmic scale. This causes the sharp downward points where the sign of temperature change switches. We omit the lower 200 m to facilitate the view of the more interesting upper section.

an order of magnitude less than strain heating (see below and Fig. 1).

Our model extends from the ice-sheet surface to 600 m depth, with uniform 6 m node spacing. Time step is 1×10^6 s (11.6 d). The density profile is measured and assumed constant, which is a reasonable assumption because long-term averages of temperature and accumulation rate do not vary significantly in the Holocene. Conductive- and advective-heat transport dominate the model, with heat generation due to densification playing a significant role in the 20–150 m depth range (see Fig. 1).

Forcings

Through time, the model is forced with surface temperatures, $T_s(t)$, calculated from isotopic ratios (Equation (8)) and accumulation rates, $\dot{b}(t)$, calculated from seasonal indicators in the ice core (Meese and others, 1992) (see Fig. 2a and b). The age scale is accurate to a year or two for the most recent times and to a few per cent for older times (Meese and others, 1992). The isotopic ratios are measured using mass spectrometry. The uncertainty in a single δ^{18}O value is less than 0.1‰. We measured ten samples per year of ice and interpolated between these to get our temperature forcing. Mean annual δ^{18}O values have an analytic uncertainty of less than 0.03‰. Note that, if our δ measurements are systematically offset from true values, the intercept (b) value in Equation (1) will be offset by the same amount in our calibration.

Inversion

Comparison of model equation solutions with measured borehole-temperature data enables us to invert for optimal values of the coefficients a and b. Δ is also treated as a free parameter in the inversion. We use a multi-dimensional form of Newton's method (Menke, 1984) to find values of model parameters that give best
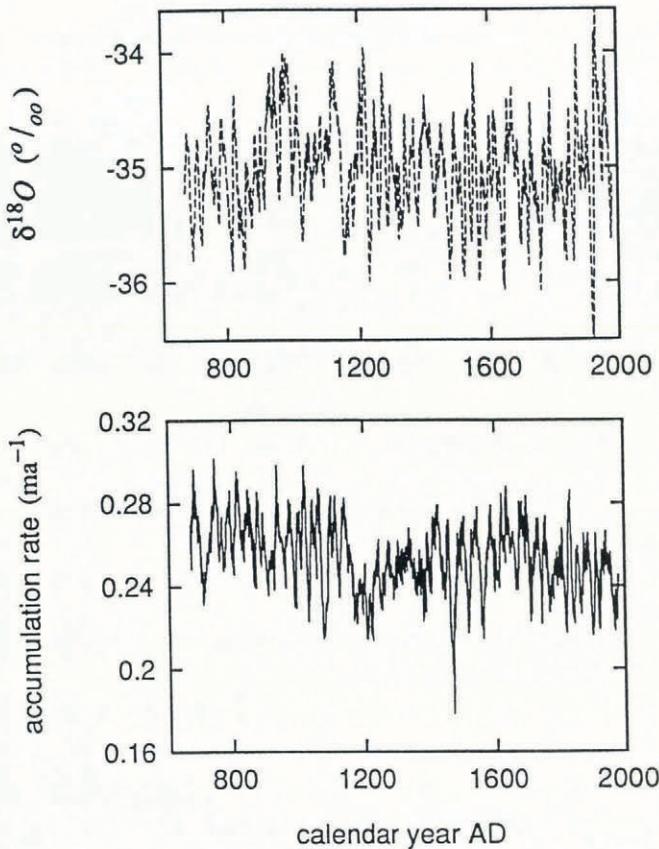
Fig. 2. *The isotope and accumulation-rate data used in our calibration, smoothed using a 10 year running average.*

agreement between model and measured temperatures, as defined by Equation (3). The inversion uses model grid points only from 36 to 216 m depth, the bottom of the measured temperature record. The top 30 m are truncated to avoid extreme sensitivity of the calibration to the most recent several years. This is desirable because the natural variability of mean annual $\delta^{18}O$ values is large; because the shallowest part of our borehole may be affected by surface winds; and because the amplitude of shallow temperature variations is huge compared to those at greater depths.

An initial guess at values for the model parameters, $m_q^0 = [a, b, \Delta]$, is changed by an amount $\hat{m}_q = [\hat{a}, \hat{b}, \hat{\Delta}]$, calculated from

$$H_{pq}\hat{m}_q = \hat{d}_p \qquad (16)$$

where $p = 1, \ldots N$ and $q = 1, \ldots M$ (N = number of grid points = 31, M = number of free-model parameters ≤ 3). Here $\hat{d}_p$ is the temperature residual, $T_p(m_q^0) - \Theta_p$, and H_{pq} is a matrix of the derivatives of T_p with respect to each model parameter, calculated numerically as

$$H_{pq} = \frac{\partial \hat{d}_q}{\partial \hat{m}_p} = \frac{T_p(m_q^0 + \hat{m}_q) - T_p(m_q^0 - \hat{m}_q)}{2\hat{m}_q} \qquad (17)$$

which we invert using singular-value decomposition to solve Equation (16). The new values $m_q^0 + \hat{m}_q$ are then modified in the same fashion with decreasing $\hat{m}_q$ until E_{ms} ceases to decrease. The inversion to solve Equation (16) is overdetermined. We neglect no eigenvalues and we find that the model resolution matrix is approximately equal to the identity matrix, with off-diagonal elements smaller than 10^{-9}.

We interpolate measured temperatures to each grid point, because the measured values have 5 m or less spacing, versus 6 m spacing for grid points. Because temperature varies gradually, this interpolation introduces insignificant error. Inversions of synthetic borehole temperatures produced by known values of a, b and Δ indicate that the numerical error of our technique is approximately $\pm 0.001‰\,°C^{-1}$ for a, $\pm 0.05‰$ for b and $\pm 0.005°C$ for Δ. In addition, the solutions do not change with variations in initial m_q^0 or with reasonable changes in the size of $\hat{m}_q$. We therefore consider our solutions to be accurate numerically.

In this paper, we map the error E_{ms} as a surface over the a–b plane. The low point of this surface, which has error E_{ms}^{min}, overlies the optimal values of the coefficients a and b, a^* and b^*. This minimum is found by using $m_q = [a, b, \Delta]$ in the inversion. Then we assign fixed values to a and use only $m_q = [b, \Delta]$. This defines a trough in the error surface that gives the best possible error for given a. It is important to define this trough because a is the parameter in our inversion of most interest to paleoclimate studies, since it relates the magnitude of variations in $\delta^{18}O$ to variations in temperature. Finally, we assign fixed values to both a and b, let $m_q = \Delta$, find the minimum E_{ms} for these (a, b) coordinates and contour the resulting surface. This surface shows how confident we can be in our calibration. If the optimal values, a^* and b^*, are well-constrained, the error surface will rise rapidly along trajectories away from the coordinate (a^*, b^*). For us to claim that (a^*, b^*) makes a significantly better paleothermometer than (a, b) at a given level of statistical confidence, the ratio $E_{ms}(a, b)/E_{ms}^{min}$ should exceed the maximum ratio of squared errors expected from random fluctuations in the data alone, which is given by the F-distribution (see Menke, 1984, p. 96–97). Thus we use an F-test that compares the surface E_{ms} to E_{ms}^{min} to outline regions in the a–b plane that contain the values of the true paleothermometer at various confidence levels. For optimal values of Δ, see Cuffey and others (1992).

Time-weighting of the calibration

If the slope and intercept of the isotope–temperature relation (Equation (1)) have changed over time, then a and b from our calibration are time-averaged values for the most recent 1340 years. Furthermore, these are weighted averages, with some times contributing more than others. For example, very recent times are weighted lightly in the calibration because we disregard the uppermost part of the borehole-temperature profile where the effects of recent temperature change are largest. We calculate the weight function, $W(\tau)$, as a semi-quantitative measure of the influence of events in each of the 1340 years on the modern borehole-temperature profile; $W(\tau)$ therefore approximates the time-weighting of a and b in our calibration.

The surface-temperature history given by Equation (1) from the 1340 year $\delta^{18}O$ record is simplified to a series of annual average perturbations about the mean, $\delta T_{av}(\tau)$, for the τth year before present. In the modern ice sheet, each $\delta T_{av}(\tau)$ will have a temperature response at depth z

$$R_z(\tau) = \Phi_z(\hat{\tau})[\delta T_{av}(\tau)]. \qquad (18)$$

Here, $\Phi_z(\hat{\tau})$ is the temperature perturbation as a function of elapsed time $\hat{\tau}$ that results from a unit forcing (1°C for 1 year) at time $\hat{\tau} = 0$. These $\Phi_z(\hat{\tau})$ are Green's functions, which we compute numerically. Note that, because τ is given as years before present, τ equals $\hat{\tau}$.

The modern temperature at depth z depends on the sum over all years of the responses $R_z(\tau)$. Comparing the magnitude of $R_z(\tau)$ for different years τ therefore gives a measure of how important each year is for determining the modern temperature structure, compared to other years, at that depth. To present this comparison graphically, incorporating all depths used in the calibration, we define the depth-averaged weight function $W(\tau)$, as

$$W(\tau) = \sum_{p=1}^{p=N} |R_{z(p)}(\tau)| \qquad (19)$$

where $z(p)$ is the depth of the pth grid point used in the calibration.

We normalize $W(\tau)$ by setting the integral of $W(\tau)$ over the entire range $0 < \tau < 1340$ years equal to unity. Then $\int_{\tau_1}^{\tau_2} W(\tau)d\tau$ gives the relative contribution of the interval $\tau_1 < \tau < \tau_2$ to the modern temperature structure and hence to the calibration of the isotopic paleothermometer.

Modern local spatial gradient of $\delta^{18}O$ with temperature

One purpose of our paper is to argue that calibrating isotopic paleothermometers using borehole temperatures is a profitable undertaking. To this end, it is useful to compare results of our borehole calibration with results of the most frequently used calibration method, that based on spatial gradients (as defined in the Introduction).

We calculate a spatial gradient using data from locations within 100 km of the GISP2 site. One of us (unpublished manuscript by J. Bolzan) has measured 10 m temperatures in the GISP2 area and collected a number of shallow cores that span approximately 25–45 years, and oxygen-isotope profiles were measured on these cores by the Geophysical Laboratory in Copenhagen (Bolzan and Strobel, 1994). Unfortunately, for logistical reasons, the isotope and temperature measurements were not made at the same sites. As a result, we interpolated the temperature field using a generalized Kriging algorithm (Olea, 1974) to generate mean annual temperatures at the shallow coring sites, except for two sites which we considered too distant from the nearest measured 10 m temperature. We then regressed isotopic values averaged over the most recent 30 year interval in the shallow cores against the interpolated mean annual temperatures. The one core that spanned only 25 years was not used.

Clausen and others (1988) measured 10 m borehole temperatures and $\delta^{18}O$ of ice cores south and east of the GISP2 site. We include these data in our correlation to widen the temperature range and increase the sample size. The isotopic data of Clausen and others (1988, fig. 4) are 30 year averages; we use the most recent value for each core. We do not use the data for Crête, because this core was drilled almost a decade before the others and

therefore does not include the late 1970s and early 1980s in the 30 year average.

RESULTS

By using the calibrated values, a^* and b^*, in Equation (8), our thermal model generates a temperature–depth profile that closely replicates the measured borehole temperatures (Fig. 3). The error surface, $E_{ms}(a,b)$, is a clearly defined narrow trough with a single minimum at $(a^* = 0.5305, b^* = -18.18)$ (Fig. 4). Here, $E_{ms}(a^*, b^*) = E_{ms}^{min} = 6.58 \times 10^{-5}$. The long axis of the trough, which follows the line

$$b = 31.47a - 34.87, \qquad (20)$$

is the direction along which the optimal values a^* and b^* are least well constrained (i.e. the trough follows an eigenvector of H_{ij}). The confidence intervals (Fig. 3), which are bounded by contours on the error surface, are roughly elliptical with the major axis much greater than the minor axis, indicating that, for a given a value, the b value is tightly constrained. The 90 and 95% confidence intervals on a are (0.453, 0.656) and (0.443, 0.689), respectively.
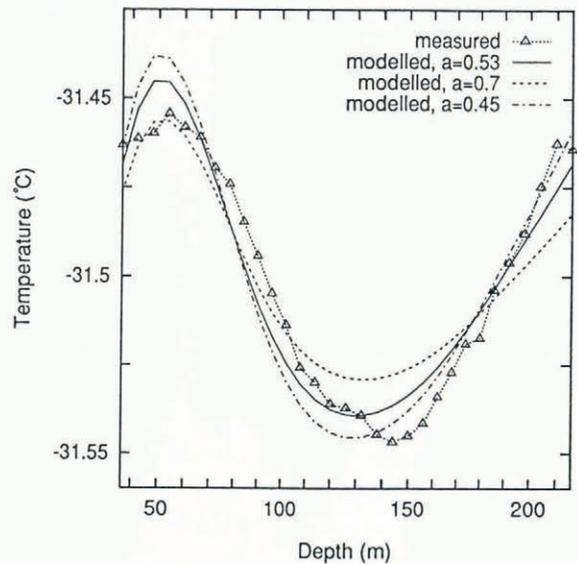
Fig. 3. Comparison of model and measured temperatures. Model results are shown for the best-fit value a = 0.53, and for the values a = 0.45 and a = 0.70, which approximately bound the 95% confidence interval for a. The b values for these calculations are given by Equation (20).

The weight function for the GISP2 $\delta^{18}O$ paleothermometer attains its peak value at 58 years BP and decays rapidly backward in time (Fig. 5) to one-third of the peak value at 300 year BP and to near zero at 1200 year BP. Our calibration is most sensitive to temperature changes of the early to mid 20th century. The median of $W(\tau)$ is the year $\tau = 259$ year BP (AD 1730). Hence, the calibration is as much determined by temperature changes occurring prior to 259 year BP as by more recent changes. Our calibration is therefore applicable to at least five or six centuries of $\delta^{18}O$ data.

The Bolzan data alone do not show a local spatial δ–T gradient (Fig. 6). Including the Clausen and others
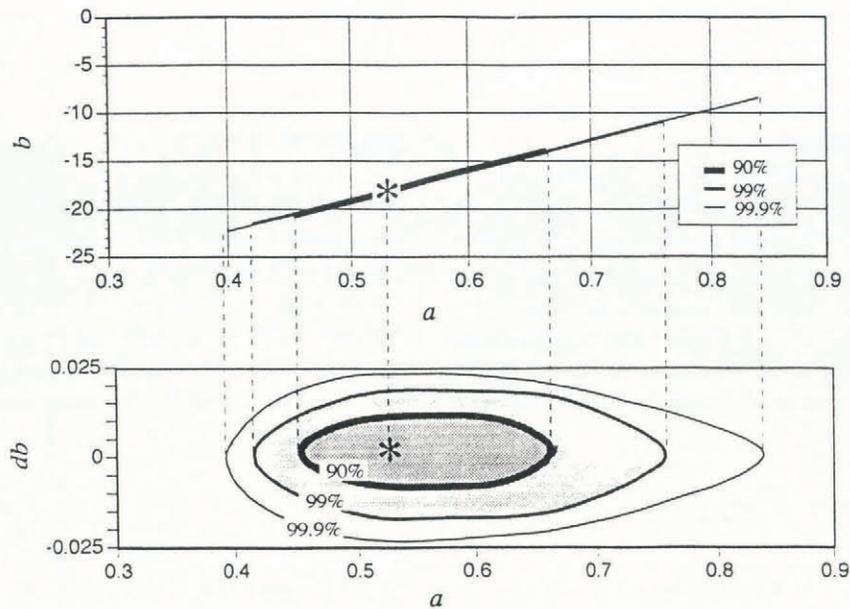
Fig. 4. Model mean-square-error surface, showing contours of 90, 99 and 99.9% confidence levels, and the best-fit value (asterisk). The intercept, b, is so closely constrained for given slope, a, that the contours appear as a line in the a–b plot in the upper panel, following Equation (20). The distance, db, of a contour from this line for given a is plotted in the lower panel.

(1988) data still shows no clearly defined δ–T gradient but, for comparison with Equation (1), linear regression gives $a = 0.47$ and $b = -20.1$. The 95% confidence interval for a is (0.17, 0.76) which is a large uncertainty compared to the uncertainty in the borehole-temperature calibration. Improving the spatial estimate would require drilling and analyzing more shallow cores.

SENSITIVITY TESTS

Methodology for the sensitivity tests

The values we use for the borehole temperatures and for some fixed parameters in our model may differ from the true values. It is important to know how this uncertainty may affect our calibration. Therefore, we test the sensitivity of the optimal values, a^* and b^*, to these uncertain model variables. We alter each model variable in question, V, by an amount $\tilde{V}$, or replace it by an alternative variable, V_{alt}, and repeat the inversion ($m_q{}^0 = [a, b, \Delta]$) using $V + \tilde{V}$ or V_{alt}. If the result has E_{ms} that is statistically significantly worse than $E_{ms}{}^{min}$, then the altered value $V + \tilde{V}$ or V_{alt} is probably physically unreasonable. Otherwise, the inversion gives new, acceptable values for a^* and b^*.

We examine the sensitivity of the calibration to:

1. The basal boundary condition. We replace the constant basal temperature T_{600}, with a constant basal heat flux implied by the steady-state initial temperature profile.
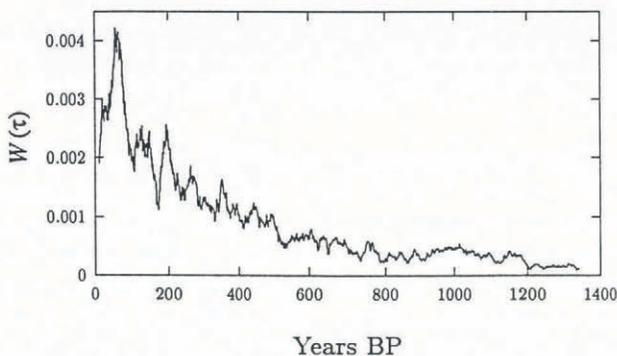
Fig. 5. The depth-averaged weight function. $W(\tau)$ for the GISP2 $\delta^{18}O$ paleothermometer. The area under the curve for a given time interval indicates the sensitivity of the modern temperature structure and the calibration to that interval. $W(\tau = 0) = 0$, because we did not use the top 30 m of the borehole in the calibration.
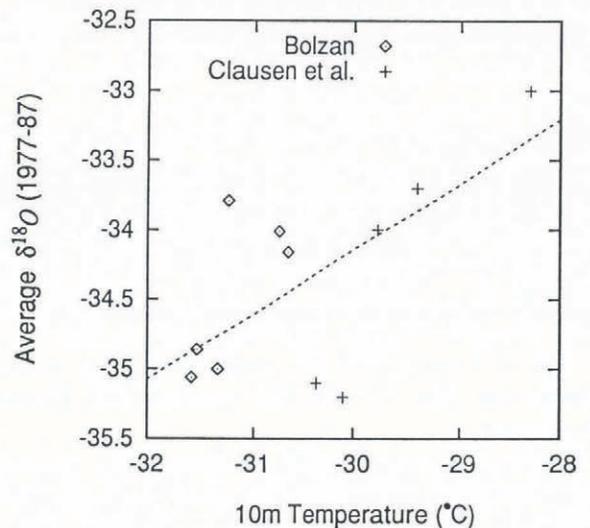
Fig. 6. The modern spatial gradient of δ and temperature from locations within 100 km of the GISP2 site, showing the Bolzan data and the Clausen and others (1988) data. There is no obvious relationship but we show the best linear fit ($\delta = 0.47T - 20.1$) for comparison with Equation (1).

2. The initial temperature profile. In Equation (5), we replace the steady-state, nearly isothermal, profile with linear profiles $T_i(z) = T_i(0) + \tilde{T}_i \frac{z}{600}$, where $\tilde{T}_i$ is the temperature difference between the 600 m depth and the surface. It is unlikely that $\tilde{T}_i < 0$ because there was a cooling trend during the late Holocene (Lamb, 1982; Dahl-Jensen and Johnsen, 1986). It is also probable that $|\tilde{T}_i|$ is less than 1°C because the difference in mean annual temperature between the climatic optimum and the first millennium AD is at most several °C (Lamb, 1982; Dahl-Jensen and Johnsen, 1986). The magnitude of the corresponding temperature maximum at depth will be considerably reduced by diffusion and the maximum will be deeper than 600 m due to advection alone. Therefore, we use $\tilde{T}_s = \pm 0.5$°C and –1.0°C as estimates of this uncertainty.

3. The thermal properties of snow. For snow of density $\rho < 750 \, \text{kg m}^{-3}$, we increase and decrease the dependence of thermal conductivity on density and temperature by the maximum amount that still approximates the data trends in figures 16 and 17 of Yen (1981). We alter the constants in Yen's equation (35), so that thermal conductivity is $0.048 \exp(0.0103T + 5.9289\rho)$ for the increased dependence case; for the decreased dependence case it is $0.100 \exp(0.0073T + 4.1456\rho)$ (units as in Yen (1981)).

4. The ice-equivalent thickness, h_i. The thickness of ice beneath Summit is uncertain by 100 m or more because of the uncertainties in velocity of radar waves through ice and the moderately coarse grid for radar surveys relative to the rough bedrock topography (Hodge and others, 1990). We have used $h_i = 3150$ m (Hodge and others, 1990). Here, we use $h_i + \tilde{h}_i$ with $\tilde{h}_i = \pm 150$ m.

5. The borehole-temperature measurements.

The absolute value
The thermistors we used are accurate to better than ± 0.1°C (Alley and Koci, 1990). For these sensitivity tests, we shift the entire temperature profile by $\tilde{\Theta}_{\text{abs}} = \pm 0.1, 0.04$ and 0.02°C.

The shape
The shape of the temperature profile was reproducible to 0.01°C. Therefore, the random error of each temperature measurement about its true value is probably less than 0.01°C in magnitude. We examine the statistically very unlikely worst-case scenario in which this error is systematically distributed such that the variation of the measured temperatures relative to their mean changes by an amount $\tilde{\Theta}_{\text{shape}} = \pm 0.01$°C. We smoothly deform the measured temperature profile so that its mean value is unchanged but so that the maximum difference between measured temperature and mean measured temperature changes by $\tilde{\Theta}_{\text{shape}}$.

Results of the sensitivity tests

Results of the sensitivity tests show that realistic uncertainties in measured temperatures and model variables do not significantly affect our calibration (see Table 1). a^* is insensitive to the basal boundary condition, the ice thickness and the absolute value of the measured borehole temperatures. It is weakly dependent on the initial temperature profile and on snow thermal properties, and more strongly dependent on systematic errors in the measured borehole-temperature trend. Because the temperature trend was highly reproducible using different measuring devices, we consider such systematic errors to be very unlikely. Assuming no such systematic error, the summed uncertainty in a^* ranges from $+0.040$ (which obtains if $\tilde{T}_s = -1.0$°C, $\tilde{h}_i = -150$ m and $\tilde{\Theta}_{\text{abs}} = +0.10$°C) to -0.038 (which obtains if $\tilde{T}_s = +0.5$°C, snow-thermal properties have minimum dependence on density and temperature, $\tilde{h}_i = +150$ m and $\tilde{\Theta}_{\text{abs}} = +0.04$°C). Thus, the sensitivity of a^* is considerably smaller than the 90% confidence interval for a^* (Fig. 4).

b^* is insensitive to the basal boundary condition and ice thickness, moderately sensitive to the absolute value of borehole temperatures and more strongly sensitive to deviations of the initial temperature profile from steady-state and to snow-thermal properties. It is most sensitive to systematic errors in measured temperatures. The summed uncertainty in b^* ranges from $+1.84$ to -0.72, assuming no systematic errors, which is much larger than the 90% confidence interval for b^* (Fig. 4).

DISCUSSION

It is clear that $\delta^{18}O$ is a useful proxy for temperature on a time-scale of decades to centuries, at the GISP2 site. There is probably no other explanation for the good fit we obtain between model and measured temperatures; we use a standard temperature model based on physical principles and a simple, widely accepted two-parameter relationship between $\delta^{18}O$ and temperature (Equation (1)). There is only one additional free parameter in the inversion, which shifts the absolute value of the initial temperature profile. From analysis of borehole temperatures at Crête and Camp Century, Johnsen (1977) and Jenssen and Campbell (1983), respectively, also concluded that $\delta^{18}O$ was a long-term proxy for temperature.

We have not tried to identify time variation in the isotope–temperature calibration using our data. Our time-independent calibration provides a sufficiently good fit of calculated to observed borehole temperatures that any improvement in fit gained by using a time-dependent calibration would be offset by the broadened confidence intervals associated with the larger number of free parameters in the model. This suggests that the calibration has not changed greatly over the most recent 1340 years for the decadal time-scale that is most important in borehole temperatures; if it had, we would not have obtained such a good fit with time-independent parameters.

The weight function provides information in addition to the time-weighting of our calibration. We can use $W(\tau)$ to estimate the calibration's sensitivity to parts of the $\delta^{18}O$ record that are suspect. For example, there is a 20 year cold period around 640 year BP for which $\delta^{18}O$

Table 1. *Tabulated results of sensitivity tests. Changing the model variables listed returned the new optimal values $a^* + \mathrm{d}a$ and $b^* + \mathrm{d}b$, where $a^* = 0.5305$, $b^* = -18.18$. Recall that the numerical error in a^* is of order ± 0.001 and in b^* is of order ± 0.05. Cases where $\mathrm{d}a$ or $\mathrm{d}b$ exceed these values are shown in bold type. Note that increasing the dependence of thermal conductivity on snow density and temperature leads to model results that are statistically unacceptable at the 95% confidence level*

		da	db
1. Basal boundary condition			
	Fixed flux instead of temperature	−0.0006	−0.017
2. Initial temperature profile	$\tilde{T}_i$	da	db
	+0.5°C	**−0.012**	**−0.36**
	−0.5°C	**+0.013**	**+0.41**
	−1.0°C	**+0.035**	**+1.08**
3. Snow thermal properties	Dependence on ρ and T	da	db
	Minimum	**−0.021**	**+0.65**
	Maximum	*No statistically acceptable model*	
4. Ice thickness	$\tilde{h}_i$	da	db
	+150 m	−0.001	−0.04
	−150 m	+0.001	+0.05
5. Borehole-temperature measurements:			
a. Uniform shift	$\tilde{\Theta}_{\mathrm{abs}}$	da	db
	+0.10°C	**+0.004**	**+0.07**
	+0.04°C	**−0.004**	**−0.15**
	+0.02°C	**+0.002**	**+0.05**
	−0.02°C	−0.001	+0.01
	−0.04°C	**+0.002**	**+0.10**
	−0.10°C	**0.002**	**+0.11**
b. Amplitude change	$\tilde{\Theta}_{\mathrm{shape}}$	da	db
	+0.10°C	**−0.095**	**−2.98**
	−0.10°C	**+0.111**	**−3.02**

values from two adjacent cores in central Greenland differ by 0.5‰ (personal communication from D. Dahl-Jensen). This discrepancy will not significantly affect our calibration because $\int W \mathrm{d}\tau \ll 1$ for this interval (Fig. 5).

Our calibrated value of the coefficient a is lower than, but similar to, previous estimates based on the spatial gradient for all of Greenland (Dansgaard and others, 1973; Robin, 1983, p. 182–84; Johnsen and others, 1989, p. 455 and fig. 3) and based on time-series analysis of data from Jakobshavn (Robin, 1983, p. 182–84). Previous estimates range from $a = 0.57$ to 0.70. This suggests that Equation (2) is not seriously in error for central Greenland, provided the spatial relationship, $\delta^{18}O$ $(T(t_0, \phi, \omega))$, is measured over a large temperature range. But the magnitude of temperature change at GISP2 during the Holocene is small compared to this range, so a *local* test of Equation (2) in the vicinity of the GISP2 site is warranted. However, our attempt to define a local spatial gradient is inconclusive (Fig. 6). This may indicate that no clear local spatial gradient exists. It certainly indicates that a lot of effort can be spent drilling shallow cores, measuring their isotopic composition and

measuring temperatures without learning anything about the $\delta^{18}O$–temperature relationship. In addition, the comparison of 10 m or 20 m temperature with decade(s)-averaged isotopes is not perfect, because the temperature at a given depth is a variably weighted average of surface temperatures over some time period. We are unsure how, in a changing climate, to average isotopes to make this comparison valid.

Given this uncertainty in what averaging time should be used, and the scatter of our data, it seems clear that the borehole calibration is an easier method for finding the δ–T relationship than is measuring spatial gradients in the vicinity of coring sites. The borehole calibration only requires measuring temperatures in the one hole drilled for the paleoclimate study, and leads to a clearly defined relationship between δ and temperature in this case. Borehole calibrations should be successful as long as the temperature profile has significant non-steady character, with deviations much larger than measurement error.

Furthermore, although the analytic uncertainty in mean annual $\delta^{18}O$ values is small, intercomparison of adjacent ice cores demonstrates a variability in mean

annual values of as much as 1.0‰, suggesting that $\delta^{18}O$ may be reliable as a thermometer only when averaged over decades or longer (e.g. Benoist and others, 1982; personal communication from D. Dahl-Jensen). Heat-transport processes provide this smoothing naturally, so borehole temperatures are well suited for calibrations of Equation (1). Moreover, the true relation between mean annual $\delta^{18}O$ and T may change with time, due to changes in the seasonality of accumulation (Fisher and others, 1983) or changes in vapor-source area and transport paths (Dansgaard and others, 1989). Borehole calibrations will give values for a and b that best average these effects over time, whereas modern spatial gradients will not include these effects at all. Unlike spatial gradient calibrations, borehole calibrations do not rely on the truth of Equation (2), which has been shown to be incorrect in at least one case (Peel and others, 1988).

CONCLUSION

For conversion of GISP2 $\delta^{18}O$ records to temperature histories, we recommend using Equation (1) with the coefficient a in the interval (0.45, 0.66), and with the corresponding b value given by Equation (2). This calibration is applicable to at least the most recent five or six centuries of isotope data.

We have shown that we can achieve a clearly defined calibration of an isotopic paleothermometer using borehole temperatures, in one case. Unlike calibrations based on other methods, borehole-temperature calibrations apply for an extended period of time at one location. For this reason and, because these calibrations require little additional cost or effort, borehole-temperature calibrations should be a regular part of ice-core paleoclimate studies that utilize isotopic paleothermometers.

ACKNOWLEDGEMENTS

REFERENCES

Alley, R. B. and B. R. Koci. 1990. Recent warming in central Greenland? *Ann. Glaciol.*, **14**, 6–8.

Alley, R.B., P.M. Grootes, D.A. Meese, A.J. Gow, K. Taylor and K.M. Cuffey. 1991. Climate at the Greenland summit: Little Ice Age to modern. *EOS*, **72**(44), 66.

Benoist, J.-P., J. Jouzel, C. Lorius, L. Merlivat and M. Pourchet. 1982. Isotope climatic record over the last 2.5 ka from Dome C, Antarctica, ice cores. *Ann. Glaciol.*, **3**, 17–22.

Bolzan, J. F. 1985. Ice flow at the Dome C ice divide based on a deep temperature profile. *J. Geophys. Res.*, **90**(D5), 8111–8124.

Bolzan, J.F. and M. Strobel. 1994. Accumulation-rate variations around Summit, Greenland. *J. Glaciol.*, **40**(134), 56–66.

Clausen, H.B., N.S. Gundestrup, S.J. Johnsen, R. Bindschadler and J. Zwally. 1988. Glaciological investigations in the Crête area, central Greenland: a search for a new deep-drilling site. *Ann. Glaciol.*, **10**, 10–15.

Cuffey, K. M., R. B. Alley, P. M. Grootes and S. Anandakrishnan. 1992. Toward using borehole temperatures to calibrate an isotopic paleothermometer in central Greenland. *Global Planet. Change*, **6**(2–4), 265–268.

Dahl-Jensen, D. and S. J. Johnsen. 1986. Paleotemperatures still exist in the Greenland Ice Sheet. *Nature*, **320**(6059), 250–252.

Dansgaard, W., S.J. Johnsen, H.B. Clausen and N. Gundestrup. 1973. Stable isotope glaciology. *Medd. Grønl.*, **197**.

Dansgaard, W., J.W.C. White and S.J. Johnsen. 1989. The abrupt termination of the Younger Dryas climate event. *Nature*, **339**(6225), 532–534.

Diment, W.H. 1967. Thermal regime of a large diameter borehole: instability of the water column and comparison of air- and water-filled conditions. *Geophysics*, **32**(4), 720–726.

Fisher, D.A., R.M. Koerner, W.S.B. Paterson, W. Dansgaard, N. Gundestrup and N. Reeh. 1983. Effect of wind scouring on climatic records from ice-core oxygen-isotope profiles. *Nature*, **301**(5897), 205–209.

Hobbs, P. V. 1974. *Ice physics*. Oxford, Clarendon Press.

Hodge, S. M., D. L. Wright, J. A. Bradley, R. W. Jacobel, N. Skou and B. Vaughn. 1990. Determination of the surface and bed topography in central Greenland. *J. Glaciol.*, **36**(122), 17–30.

Jenssen, D. and J. A. Campbell. 1983. Analysis of temperature, isotopic and total gas content profiles. Heat conduction studies. *In* Robin, G. de Q., *ed. The climatic record in polar ice sheets*. Cambridge, Cambridge University Press, 125–138.

Johnsen, S.J. 1977. Stable isotope profiles compared with temperature profiles in firn with historical temperature records. *International Association of Hydrological Sciences Publication* 118. (Symposium at Grenoble 1975 — *Isotopes and Impurities in Snow and Ice*), 388–392.

Johnsen, S.J., W. Dansgaard and J.W.C. White. 1989. The origin of Arctic precipitation under present and glacial conditions. *Tellus*, **41B**(4), 452–468.

Jouzel, J. and L. Merlivat. 1984. Deuterium and oxygen 18 in precipitation: modelling of the isotopic effect during snow formation. *J. Geophys. Res.*, **89**(D7), 11,749–11,757.

Lamb, H. H. 1982. *Climate, history and the modern world*. London and New York, Methuen & Co. Ltd.

Malvern, L. E. 1969. *Introduction to the mechanics of a continuous medium*. Engelwood Cliffs, New Jersey, Prentice-Hall.

Meese, D.A., A.J. Gow, R.B. Alley, K. Taylor and M. Ram. 1992. Variations in accumulation and their relationship to known climatic change as determined in the top 719 m of the GISP2 core. *EOS*, **73**(43), Supplement, 175.

Menke, W. 1984. *Geophysical data analysis: discrete inverse theory*. Orlando, Florida, Academic Press.

Olea, R. A. 1974. Optimal contour mapping using universal kriging. *J. Geophys. Res.*, **79**(5), 695–702.

Paterson, W.S.B. 1981. *The physics of glaciers. Second edition*. Oxford, etc., Pergamon Press.

Paterson, W.S.B. and G.K.C. Clarke. 1978. Comparison of theoretical and observed temperature profiles in Devon Island ice cap, Canada. *Geophys. J. R. Astron. Soc.*, **55**, 615–632.

Peel, D.A., R. Mulvaney and B.M. Davison. 1988. Stable-isotope/air-temperature relationships in ice cores from Dolleman Island and the Palmer Land plateau, Antarctic Peninsula. *Ann. Glaciol.*, **10**, 130–136.

Robin, G. de Q. 1983. The climatic record from ice cores. *In* Robin, G. de Q., *ed. The climatic record in polar ice sheets*. Cambridge, etc., Cambridge University Press, 180–195.

Sanderson, T.J.O. 1977. An error in ice-temperature measurement. *J. Glaciol.*, **18**(79), 329–333.

Yen, Y.-C. 1981. Review of thermal properties of snow, ice and sea ice. *CRREL Rep.* 81-10.

The accuracy of references in the text and in this list is the responsibility of the authors, to whom queries should be addressed.